Effect of Phase Transition Temperature and Thermal Conductivity on the Performance of Latent Heat Storage System

Yu Bie [1, 2], Ming Li [1, *], Reza Malekian [3], Fei Chen [2], Zhikang Feng [1], Zhixiong Li [4, 5]

1   Solar Energy Research Institute, Yunnan Normal University, Kunming 650500, China;

2   Faculty of Chemical Engineering，Kunming University of Science and Technology, Kunming 650500, China;

3   Department of Electrical, Electronic and Computer Engineering, University of Pretoria, Pretoria 0002, South Africa;

4   School of Mechatronics Engineering, China University of Mining and Technology, Xuzhou 221116, China

5   School of Mechanical, Materials, Mechatronic and Biomedical Engineering, University of Wollongong, Wollongong, NSW 2522, Australia

A b s t r a c t： The heat transfer properties of phase change materials (PCMs) are of importance for the efficiency assessment on the heat storage and release in solar thermal systems. Previous research results demonstrate that the increase of thermal conductivity of PCMs can enhance the thermal performance in solar thermal systems; however, the corresponding mechanism is not clear. To this end, this work investigates the influence of PCMs properties on storage performance of solar thermal systems. First, experimental testing was conducted to verify the effectiveness of a thermal simulation model in the heat storage and release process. Then, the proposed simulation model was used to investigate the performance of several commonly used PCMs in the process of melting and solidification. The influence of thermal conductivity and phase transition temperature on the thermal storage properties was analyzed. The analysis results demonstrated that the influence of phase transition temperature on the thermal system performance was greater than that of the thermal conductivity in short time, while the thermal conductivity contributed greater influence on the system performance in long time. The phase transition temperature hardly affected the total system efficiency if given enough heat transfer time. The findings in this work may provide a theoretical reference for the selection of heat storage materials.

----

[*] Corresponding author. Tel.: +86 871 65517266.
 E-mail address: lmllldy@126.com (M. Li).

1 *Keywords*: Thermal storage materials; Heat transfer performance; Phase transition temperature; Thermal

2 conductivity

3

4 **Nomenclature**

5 E quantity of exergy, kJ

6 C specific heat capacity, kJ/(kg·K)

7 $\dot{E}$ exergy transfer rate, W

8 f mass fraction of liquid phase

9 L latent heat, kJ/kg

10 Q quantity of heat transfer, kJ

11 t temperature, ℃

12 h specific enthalpy value, kJ/kg

13 m mass, kg

14 $\dot{Q}$ heat transfer rate, W

15 T t+273.15, K

16 *Greek symbols*

17 ρ density, kg/m^3

18 μ dynamic viscosity, kg/(m·s)

19 τ time, s

20 φ ratio

21 λ thermal conductivity, W/(m·K)

22 β thermal expansion coefficient, K^{-1}

23 $\varDelta$ difference value

24 δ differential value

25 *Subscript*

26 m melting

27 *St*   stored

28 *max*   maximum

29 S solid state

30 *0,1,2*   the initial and other two states

31 f working fluid

32 P pressure

33 *re*   released

34 l liquid state

35 *loss*   the heat lost

36 *Abbreviation*

37 PCM   phase change material

38 SIPH   solar industrial process heating

39 LHTES   latent heat thermal energy storage

40 HTF   heat transfer fluid

41 ET   experimental temperature

42 ST   simulated temperature

1. Introduction

The energy consumption due to thermal loads in industrial productions accounts for 15% to 30% of the total energy consumption in many countries [1]. In order to reduce the greenhouse gas emission and save energy, renewable energies (e.g., solar energy) become one of the significant orientations in instead of traditional fossil energy. Among the solar utilization, the solar thermal utilization, such as a solar industrial process heating (SIPH) system, in medium temperature matches the industrial heat load well, such as low-pressure vapor or hot air within the temperature range of 100~250°C [2]. The SIPH system in medium temperature are usually composed of one solar collecting device, one heat storage device and one heat exchanging device. The heat storage device that can overcome the intermittency and instability of solar heat supply is connected with the other two devices, thus its performance directly influences the thermal utilization system. To ensure high performance of the heat storage device, the latent heat storage has been widely adopted in the SIPH systems in recent years. Therefore, the properties and characteristics of PCMs used in the latent heat storage have attracted considerable attentions [3].

In terms of PCM type, the organic compounds and salt hydrates are suitable for the heat load under 100°C, and the eutectic molten salts fit the heat load with temperature range from 100 to 250°C. So the eutectic molten salts have been extensively used in SIPH thanks to its suitable temperature range, high latent heat and heat storage density [4]. Up to now, lots of researches focus on the enhancement of the low thermal conductivity (nearly 0.5W/m·K) of the eutectic molten salt materials. This is because low thermal conductivity may lead to a poor heat conduction performance, a low heat transfer rate, and long heat storage/release time [5]. Solutions, such as adding additives, positioning fixed, stationary high conductivity inserts or arranging metal skeleton, fins or honeycomb, have been introduced to enhance the thermal conductivity of the eutectic molten salt materials [6]. Specifically, recent advances focus on the addition of

1 expanded graphite (EG) [7-10], carbon fiber [11-13], metal foam and powder [14-16], and preparation of

2 micro-nano composite [17-20]. Wang et al. [9] put forward a kind of phase change composites with

3 double-layer carbon network structure and found that when the EG reaches 20 wt%, the thermal conductivity

4 could be increased to 7.5 times compared with the original paraffin. Fukai et al. [11] studied the

5 enhancement effect of adding random carbon fiber and carbon fiber brush on paraffin thermal conductivity

6 and found that the effect of carbon fiber brush was significant. Zhang et al. [14] analyzed the melting and

7 solidification process with and without the metal foam in molten salt, and it shows that increasing the copper

8 foam and nickel foam could shorten the solidification time by 28.8% and 19.3%, respectively. Das et al.

9 [19-20] carried out the numerical simulation analyzing of the melting process of organic paraffin in a

10 horizontal tube shell latent heat storage device, and the results reveal that adding the nanocomposite can

11 promote the thermal conductivity of PCM to a certain extent. When 1 vol% nanometer materials with various

12 dimensionalities were added into the same PCM, the melting rate only increases by 2% as for spherical

13 nanoparticles addition; however, the melting rate would increase 27% or 40% respectively for inclusion of

14 single-walled carbon nanotubes or graphite nanoplatelets, and the total melting time would be reduced by

15 15% or 25%.

16   Literature review indicates that the thermal conductivity enhancement can help to rise the energy storing

17 and releasing rate, reduce the melting and solidifying time correspondingly, and improve the heat storage

18 efficiency. Furthermore, the driven temperature difference needed to absorb and release the same heat is

19 smaller because of higher heat transfer capability. However, the increase of thermal conductivity not only

20 increases the cost of materials, but also reduces the effective storage volume and shortens the service life. In

21 addition, the enhancement of thermal conductivity might not always lead to more stored heat energy and

22 exergy under a certain condition of heat source during given storing time, which are also definitely the

1   important indicators of thermal performance.

2   The latest study showed that choosing appropriate phase change temperature could compensate the

3   stored energy and exergy in a certain degree [21]. Researchers have explored the optimum melting

4   temperature according to the given heat source and cold source from the perspective of the second law of

5   thermodynamics. Bjurström et al. [22] considered that from an exergetic point of view, the optimal phase

6   transition temperature could be recognized as geometric mean of the charging and the initial temperature.

7   The melting temperature is expected to be low when the end temperature of heat storage is fixed while it

8   expected to be high considering a high exergy content during heat release process. Therefore, the optimum

9   phase transition temperature can be obtained to reach the minimum irreversibility.

10   Compared with the single PCM, using multiple cascade PCMs along the flow path of hot fluid can

11   make an increase in the overall stored energy and exergy [23-26]. Gong et al. [23] arranged two, three, and

12   five PCMs for a heat storage device and found that the stored exergy is 33.1%, 42.2% and 47.7% more than

13   that of a single PCM, respectively. In addition, the heat transfer rate can be also affected because of the

14   temperature difference of heat transfer. For example, Farid [27] conducted a comparison between three

15   different melting point PCMs and a single PCM, and the results showed that the heat transfer rate increased

16   by 15% using the three PCMs. It believes that the transition temperature strongly affects the overall heat

17   energy and exergy storage. The optimal phase transition temperature is involved with the performance target

18   of minimum irreversibility and maximum exergy efficiency. Multistage cascade PCMs heat storage can

19   promote the quantity and efficiency of exergy, but the effect is not obvious increased as more than three

20   PCMs.

21   To sum up, the influence of thermal conductivity or phase transition temperature on SIPH performance

22   has been studied separately in the past decade. However, to our best knowledge, very limited researches have

considered the combined effect of these two factors on the actual heat charging and discharging

characteristics. Note in [28] that the metal foam has obvious reinforcement of the discharging process but

little enhancement of charging process. The reason is probably that the metal skeleton has restrained the

natural convection effect in the melting process. While it is known that the start of natural convection mainly

depends on the melting temperature, the influence of thermal conductivity should be considered with the

transition temperature.

To address the aforementioned issue, this work aims to investigate the combined effect of thermal

conductivity and phase transition temperature on SIPH performance. A numerical simulation model was

developed for this purpose. The comparison between the numerical simulation and experimental testing was

firstly carried out to examine the numerical model in the molten salt melting and solidification simulation.

Then the simulations of heat storage and release process were performed to learn the influence mechanisms

of the combined effect of thermal conductivity and phase transition temperature on SIPH performance. The

contributions of this research may add new insight in understanding the enhancement of PCMs on SIPH

performance and provide theoretical reference for the selection of heat storage materials in solar energy.

The rest of the article is organized as follows. In the second section, a numerical simulation model was

introduced and the simulation results were compared with experimental data. In the third section, the analysis

of the influence of the phase transition temperature and thermal conductivity on the performance of heat

storage system was implemented. the conclusions were drawn in the fourth section.

2. Validation of numerical simulation process

In order to reduce the time and operating cost, this paper adopts numerical simulation to investigate the

combined effect of thermal conductivity and phase transition temperature on SIPH performance. A

simulation model is established to explore the influence of material physical parameters on various heat

1   storage and release performance.

2   **2.1 The introduction of experimental platform and simulation model establishment**

3   The experimental platform is constructed based on a heat transfer fluid (HTF) tank, an electric heating

4   control system, a latent heat thermal energy storage system (LHTES) tank and the connecting pipes. The

5   structure diagram of the test platform is shown in Fig. 1. The LHTES is a tube-shell heat exchanger, with the

6   HTF running in the tube-side and PCM filling for 80% volume in the shell-side, and with the peripheral

7   adiabatic treatment. In order to enhance the heat transfer, a number of annular fins are evenly arranged on the

8   outer edge of the tube. For the sake of testing temperature of the PCM in real time, a temperature probe is

9   installed in the tank.

10   In addition, the temperatures of the thermal oil in different locations are monitored in real time to ensure

11   the normal operation of the temperature control system. Six temperature probes (i.e., Pt100 thermal

12   resistance temperature probes) are arranged at the location of A ~ F shown in the left of Fig. 1, and a

13   16-channel paperless recorder is used for real-time recording.
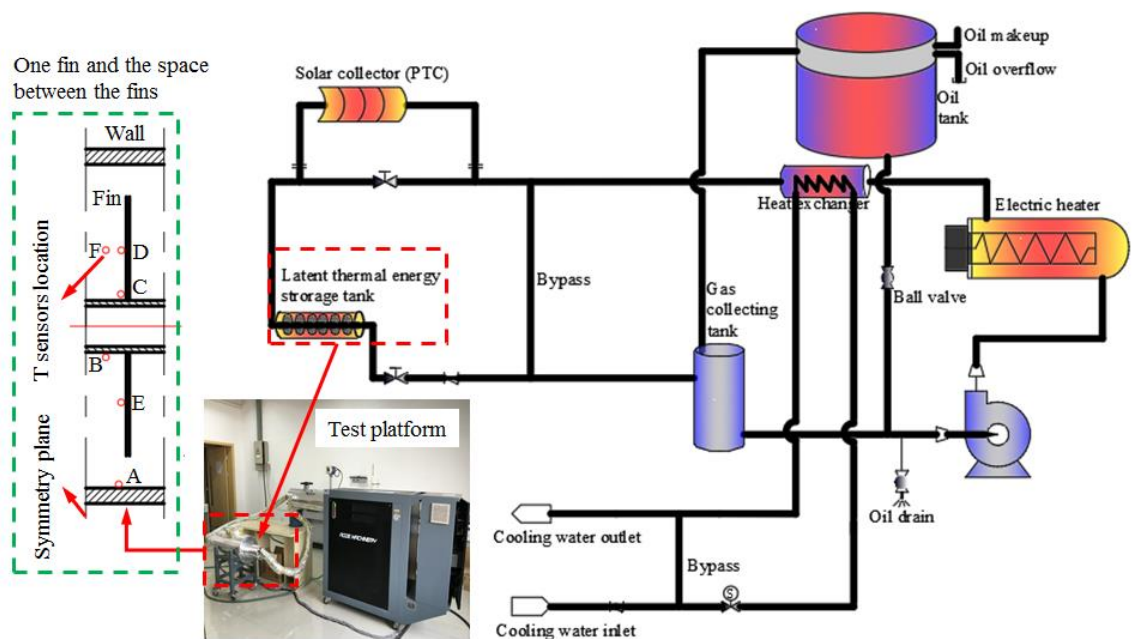
14

15   Fig. 1. Structure diagram of latent heat thermal energy storage experimental platform.

1   Experimental scheme is as follows. During the melting stage, the HTF temperature keeps stable in the

2   vicinity of 270 °C as a constant heat source, merely because the upstream concentrated solar field gain might

3   make the HTF temperature in range of 250 ~ 300 °C. The temperature can be adjusted by the electric heater

4   power, and PCM in the LHTES should store thermal energy continuously until all the monitored

5   temperatures are above the melting point. During the solidification stage, the thermal load is used to make

6   the feedwater, which is preheated to 70 °C to function as the low-pressure steam. The monitored

7   temperatures were recorded throughout the solidification process. The indoor experimental was carried out

8   under the ambient temperature of 25 °C.

9   A simulation model corresponding to the experimental platform with necessary simplifications was then

10   established. It assumed that the constant HTF temperature does not decay when it flows through the heat

11   storage tank with length of 500 mm. Along the LHTES tank length, there are fourteen fins evenly arranged

12   every 34 mm with a thickness of 2 mm. Because the heat transfer space is periodic along the axial direction

13   of the pipeline, and the left and right sides of the shell are symmetrical, the physical model of the LHTES in

14   Fig. 1 can be simplified into a symmetrical three-dimension (3D) finite model (see Fig. 2). A half part of the

15   3D model at the right side between the two mean lines of adjacent fins along axial direction was selected as

16   the calculation domain, that is, a half of a fin and a half of the two fins spacing were included in the

17   calculation domain. Then the commercial software ICEM was employed to mesh the calculation domain

18   into 18660 hexahedral grids based on the grid independence verification and compromise between the

19   computing efficiency and accuracy. The detailed grid structure and grid quality analysis are also shown in
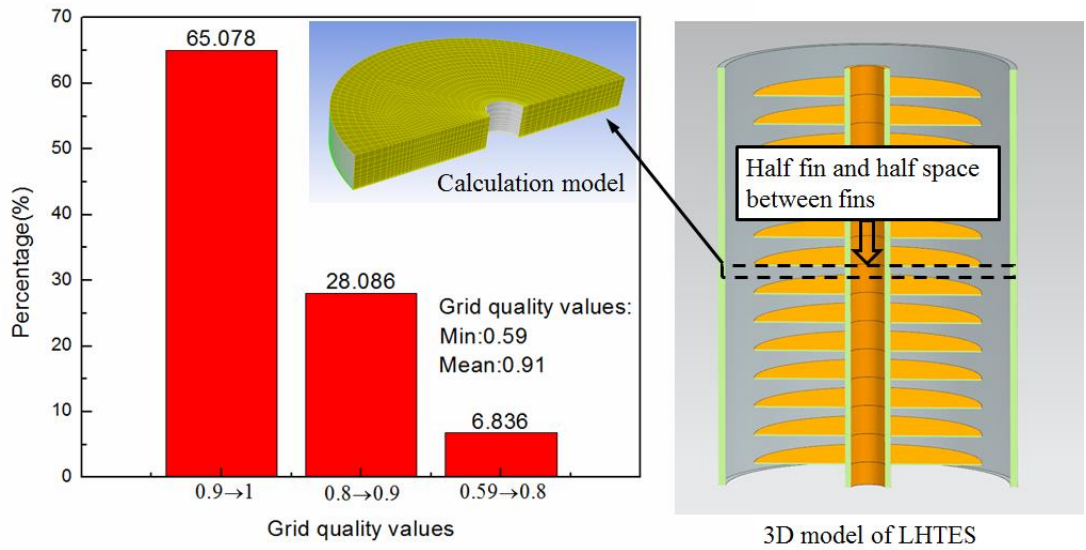
20   Fig. 2.

Fig. 2. 3D model of LHTES and grid quality analysis of calculation model.

In the numerical simulations, the following imperative assumptions are made.

(1) The fluid in the liquid phase is incompressible Newtonian fluid and the Boussinesq hypothesis is applicable. When natural convection starting, it is merely under the condition of laminar flow.

(2) The fluid surface tension is negligible, and the volume change of molten salt during the phase transition is negligible.

(3) The temperature of the HTF is assumed to be a constant, and the temperature of inner wall of the tube is regarded to be a constant as well because the heat transfer resistance of HTF and the inner tube wall can be negligible.

The commercial CFD software ANSYS 15.0/Fluent was adopted to implement the simulations and the build-in formulation of enthalpy-porosity is used to make the control equations uniform both for solid and liquid phase. Correspondingly, the 3D double-precision, unsteady solver, solidification/melting model and the time step of 0.02 s were selected for the calcualtion.

1 **2.2 Material selection and boundary conditions for the simulations**

2   The materials of phase change energy storage used in this study are two typical PMCs close to the

3   composition of solar salt and Hitec salts, which are widely used in the solar thermal electricity. One is the

4   composite molten salt (PCM1) [28] consisting of 50 wt% $NaNO_3$ and 50 wt% KNO_3, and the other (PCM2)

5   is based on the Hitec salt with additives added in the composition of the ternary nitrate [29]. The Physical

6   properties of selected PMCs are listed in Table 1.

7   Due to that both the thermal conductivity and the phase transition temperature have significant effects

8   on melting and solidification characteristics, it is necessary to triple the thermal conductivity of PCM1 to

9   form a new material PCM1+. The thermal conductivity of PCM1+ is quite close to that of the PCM2. It can be

10   noticed from the introduction section that the thermal conductivity can be improved by 30 times, so it is

11   feasible to triple the thermal conductivity theoretically and practically. In the setting parameters of the

12   materials, the thermal conductivity λ and specific heat capacity C_P at constant pressure were set for the

13   piecewise function.

14   Table 1. Thermophysical properties of PCMs

Parameters	(PCM1/PCM1+) Value		(PCM2) Value	
ρ (kg/m^3)	Solid state	2079.0	Solid state	2130
	liquid state	1884.0	liquid state	2081.2
t_m (°C)	melting	218~228	melting	137~140
	solidification	215~225	solidification	140~143
L (kJ/kg)	122.89		52.3	
λ (W/(m·K))	Solid state	0.705 / 2.115*	1.3(T ≤100°C)	
	liquid state	0.478 / 1.434*	2.0484(100°C <T ≤150°C) 1.4289(T>150°C)	
C_P (kJ/kg·K)	1.05(T≤90°C) 1.85(90°C<T≤228°C） 1.50(T>228°C)		2.13(T≤90°C) 3.89 (90°C< T ≤ 228°C） 2.50 (T >228°C)	
μ (kg/(m·s))	0.00506		0.00301	

β (K$^-$)	melting	5.47×10^{-5}	melting	2.6×10^{-4}
	solidification	7.06×10^{-5}	solidification	9.7×10^{-6}

1   * denotes the values especially for PCM1$^+$, and other properties is the same as PCM1.

2   The PCMs melting and solidification processes were numerically calculated under the following

3   boundary conditions. The left and right surfaces are symmetrical boundaries, and the outer contour interface

4   is the adiabatic boundary. The heat exchange surface between the PCM and the heat tubes and fins are the

5   coupling boundary at which the temperature and the heat flux are continuous. As for the initial conditions,

6   the temperature inside the PCM area is consistent at the start of the two processes. The initial melting

7   temperature is 25°C and the temperature in the solidification process is 250°C.

8   **2.3 Numerical simulation and experiment validation**

9   The phase transition temperature was calculated in the numerical simulations. The mass fraction of liquid

10   phase and the temperature contours in the melting process in the plane of fin are described in Fig. 3. The

11   simulated temperatures at the locations A~F in the melting and solidification processes were then compared

12   with the experimental results. The temperatures of PCM1 in the melting and solidification processes were

13   recorded every 15 minutes at the locations A~F in the experiments. The comparison results between the

14   simulation temperature (ST) and the experimental temperature (ET) in the melting process are depicted in

15   Fig. 4.

16
17   (a) Mass fraction of liquid phase contours   (b) Temperature contours
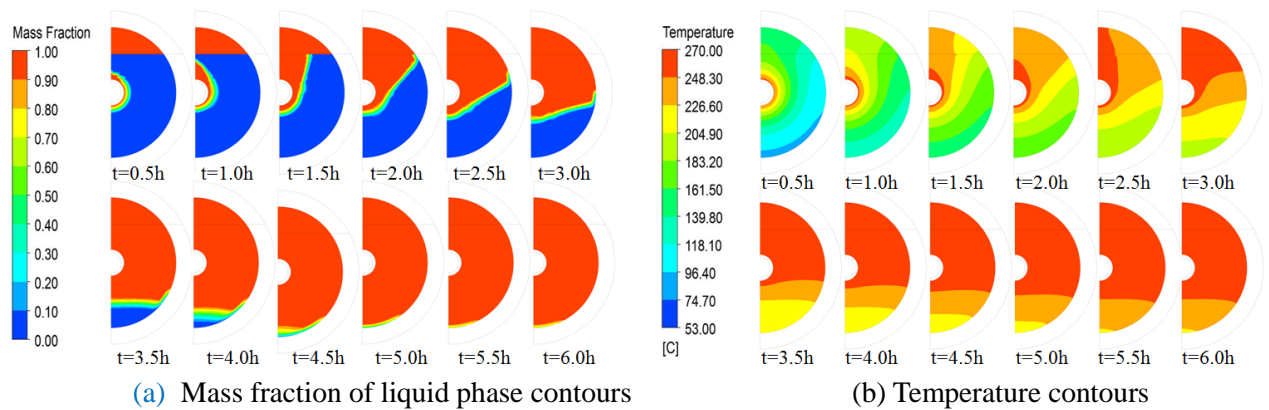
18   Fig. 3. Results during melting process.

1   It can be seen from Fig. 4(a) that the trend of ET and ST curves are monotone increasing in every

2   location. The ET is smaller than ST due to heat loss in the experiments. At location A, the inner temperature

3   field of the tank and the heat loss of the wall in simulation affect the temperature. At location B, the

4   temperature is influenced by the pipe temperature. At locations C, D and E, the temperatures are affected by

5   the fin's temperature and the free convection. At location F, the temperature is affected by the free convection

6   and the air temperature. In the starting time, the temperature increasing trends at different locations are

7   different, especially at locations D and F. With the increasing temperature of the air and the influence of the

8   free convection, the temperature at location F increases markedly compared with location D. In the melting

9   process, the temperature curves at locations D and B are almost the same.

10   As can be seen from Fig. 4(b), the errors between ET and ST at the six locations are very close to each

11   other and the maximum error is 9.5%. This means, in melting process the temperature field affected by the

12   heat loss is offset. So the simulation accuracy of the melting process is acceptable.
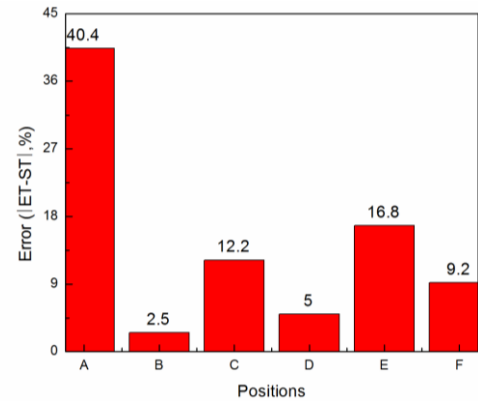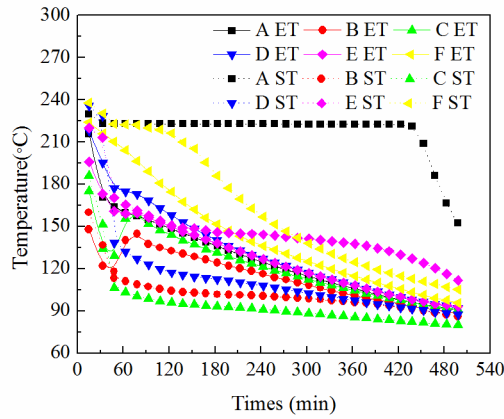

13
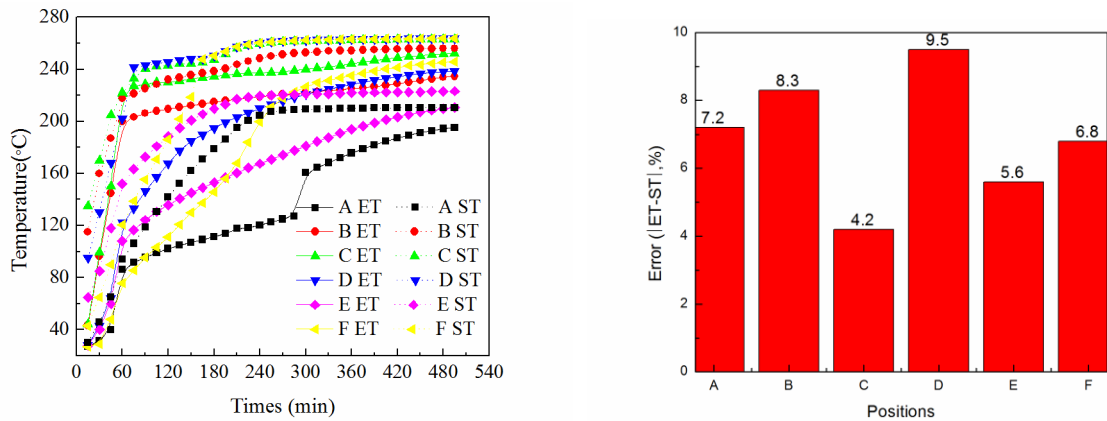
14   (a)Temperature   (b) Errors between ET and ST

15   Fig.4. Results during melting process at the locations A~F.

16   The comparison results during solidification process are provided in Fig. 5. As can be in the figure, the

17   heat transfer mechanism of the solidification process is similar to that of the melting process. The difference

18   is that there presents a supercooling phenomenon at the beginning time in solidification process, resulting in

19   a large error between the ET and ST in Fig. 5(b) at location A. In addition, in Fig. 5(b) the error between ET

20   and ST at location E is larger than those at other locations. The reason is probably caused by the heat loss

21   and the temperatures at location C and D, where hot air can be kept. Based on the comparison results, the

22   changeable rule of the temperature in solidification is credible.
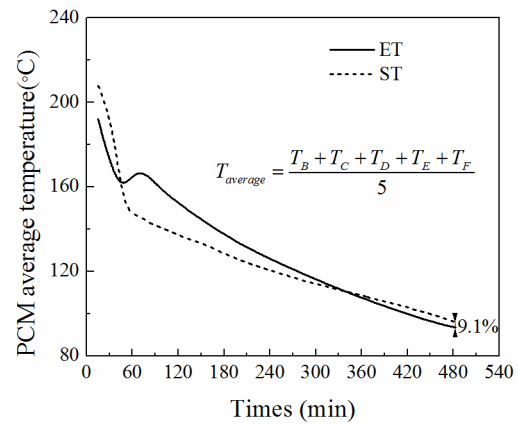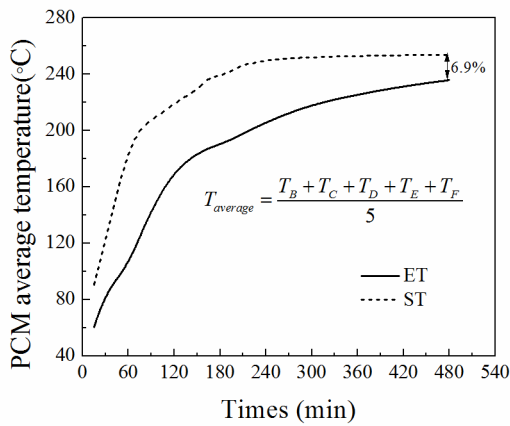
(a)Temperature   (b) Error between ET and ST

Fig. 5. Results during solidification process at the location A~F.

Fig. 6 manifests the error curves of the average temperature at locations B, C, D, E and F between ET and ST. It can be seen in the figure that the simulated average temperature is very close to the experimental result. The error in the   melting process is 6.9% once the system enters into stable operating condition while in the stable solidification condition the error is 9.1%. Therefore, the established simulation model can be used to investigate the combined effect of thermal conductivity and phase transition temperature on SIPH performance.

(a) Melting process   (b) Solidification process

Fig. 6. Comparison results of the average temperature between ET and ST

3. Effect of phase change temperature and thermal conductivity thermal transfer

3.1 The evaluation index of numerical simulation process

13

The evaluation indicators for the thermal conductivity of phase change thermal storage materials in this work adopt the heat transfer rate indicator, efficiency indicator, energy analysis and exergy analysis. The common evaluation indexes are listed below [30, 31].

The complete charging/discharging time of heat storage/release process is defined as the total time to complete the phase change process from the initial state. Heat storage ratio is a ratio value between the heat storage within the above time to the available maximum heat storage given limitless time, as shown in Eqs. (1) ~ (4).

$$\phi_{st} = \frac{\int \dot{Q}_{st} d\tau}{Q_{st\_max}} = \frac{Q_{st}}{Q_{st\_m}}$$

(1)

$$Q_{st\_max} = m \cdot [C_s \cdot (t_m - t_0) + f \cdot \Delta h_m + C_l \cdot (t_e - t_m)]$$

(2)

$$\phi_{re} = \frac{\int \dot{Q}_{re} d\tau}{Q_{re\_max}} = \frac{Q_{re}}{Q_{re\_max}}$$

(3)

$$Q_{re\_max} = m \cdot [C_l \cdot (t_0 - t_m) + f \cdot \Delta h_m + C_s \cdot (t_m - t_e)]$$

(4)

Thermal energy storage/release efficiency characterizes the relationship between heat storage or heat release and heat loss, as shown in Eqs. (5) and (6).

Thermal energy storage efficiency is defined as:

$$\eta_{st} = \frac{\int \dot{Q}_{st} d\tau}{\int \dot{Q}_{su} d\tau} = \frac{Q_{st}}{Q_{su}} = \frac{Q_{st}}{Q_{st} + Q_{loss}}$$

(5)

Thermal energy release efficiency is defined as:

$$\eta_{re} = \frac{\int \dot{Q}_{re} d\tau}{\int \dot{Q}_{st} d\tau} = \frac{Q_{re}}{Q_{st}} = \frac{Q_{re}}{Q_{re} + Q_{loss}}$$

(6)

The total heat loss includes the heat loss of the HTF during the flow and the heat loss of the LHTES unit itself. The LHTES heat loss includes radiation and air convection heat loss. In the case the temperature inside the tank is given, the relation formula of LHTES heat loss and heat storage tank wall temperature can be expressed as

1
$$\dot{Q}_{loss}=0.326t_w\text{-}17.686 \qquad (7)$$

2   In order to further evaluate the quality of stored and released thermal energy, Eqs. (8) and (9) are used

3   to calculate the exergy analysis.

4
$$\delta E_x = (1-\frac{T_0}{T})\delta Q \qquad (8)$$

5
$$E_x = m\cdot\int_{T_1}^{T_2}(1-\frac{T_0}{T})C_p dT \qquad (9)$$

6   The corresponding storage/release exergy ratio can be found by

7
$$\phi_{ex\_st} = \frac{\int \dot{E}_{st}d\tau}{\dot{E}_{st\_max}} = \frac{E_{st}}{E_{st\_max}} \qquad (10)$$

8
$$\phi_{ex\_re} = \frac{\int \dot{E}_{re}d\tau}{\dot{E}_{re\_max}} = \frac{E_{re}}{E_{re\_max}} \qquad (11)$$

9   The thermal storage performance of PCM1, PCM2 and PCM1^{+} are compared respectively from four

10   aspects of the total heat storage time, the heat transfer power, the heat storage efficiency and the heat storage

11   rate in the heat storage duration. The comparative analysis provides a priority between thermal conductivity

12   improvement and the phase transition temperature enhancement.

13   **3.2 The melting process**

14   **3.2.1 Complete charging time**

15   The average mass fraction of liquid phase was adopted to describe the liquid phase of the materials in

16   the melting or solidification process. The average mass fraction variation of liquid phase with charging time

17   for the three PCMs in the heat storage process is shown in Fig. 7.

18   It is can be seen from Fig. 7 that, PCM2 only needs 90 minutes to melt while PCM1 takes about 450

19   minutes to complete the melting process. When the thermal conductivity of PCM1 is increased to PCM1^{+},

1   the melting time is 270 minutes, shortened by 40% against PCM1. The thermal response obviously

2   accelerates using PCM1$^+$, but the melting time is still longer than that using PCM2.
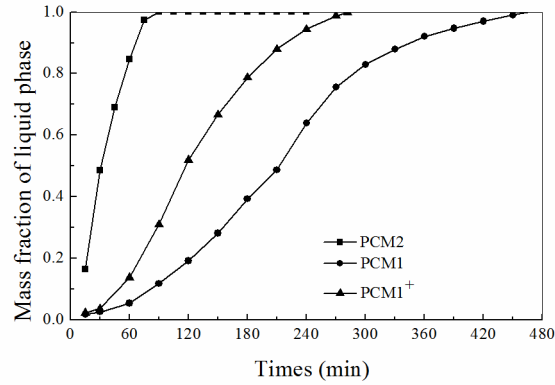
3

4   Fig. 7. Mass fraction of liquid fraction variation during melting process.

5   **3.2.2 thermal energy storage efficiency and ratio**

6   The heat flux variations from inner wall during charging process for the three PCMs are shown in Fig. 8.

7   It can be seen from Fig. 8. that the heat transfer power of PCM2 is far higher than that of PCM1 in the early

8   stage of melting, and as the temperature difference of heat transfer decreases, the heat transfer power of

9   PCM2 gradually decreases to a lower level than PCM1 after about 100 minutes. Because the temperature has

10 gradually approached to the heat source temperature, the temperature difference of the PCMs decreases after

11 the completion of the phase change process. The performance of PCM1$^+$ is consistent with PCM2, and its

12 initial efficiency is relatively lower than PCM2 but higher than PCM1.
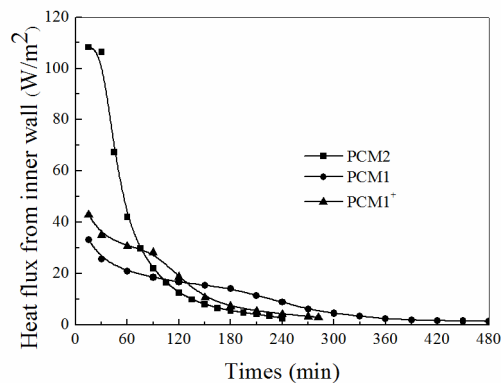
13

14   Fig. 8. Heat flux variation from inner wall variation during melting process.

16

1   According to the results in Figs. 7 and 8, comparative analysis between the three PCMs with respect to

2   the total heat storage, heat loss, maximum heat storage and the corresponding heat storage efficiency within

3   90 and 270 minutes is provided in Tables 2 and 3.

4   Table 2. Calculated thermal energy storage and loss results within 90 min

Material	Tot. stored (MJ)	Heat loss (MJ)	Max. stored (MJ)	Energy efficiency	Energy storage ratio
PCM1	5.461	0.581	12.430	0.894	0.439
PCM2	15.541	0.633	19.041	0.959	0.816
PCM1$^+$	7.814	0.634	12.430	0.919	0.629

5

6   Table 3. Calculated thermal energy storage and loss results within 270 min

| Material	Tot. stored (MJ)	Heat loss (MJ)	Max. stored (MJ)	Energy efficiency	Energy storage ratio
PCM1	10.660	1.988	12.430	0.814	0.858
PCM2	18.222	2.269	19.042	0.875	0.957
PCM1$^+$	11.630	2.191	12.430	0.812	0.936

7   It should be noted that, due to the uneven temperature distribution in the heat storage tank, the wall

8   temperature of the heat storage tank is also uneven, and the calculation of the heat loss is equal to the

9   weighted average temperature of the molten salt mass. When calculating the total heat storage, the mass of

10   PCM1 and PCM1$^+$ should be 24.40 kg filled in the experiment, and the mass of PCM2 should be 26.95 kg in

11   the same liquid volume as the former.

12   As seen from Tables 2 and 3, PCM2 stores more heat in the same time than PCM1 and PCM1$^+$, but the

13   heat loss is not significantly different. When all the materials reach the same temperature, the total energy

14   storage of PCM2 is more than those of PCM1 and PCM1$^+$ while PCM1 and PCM1$^+$ store the same amount.

15   This means that the thermal conductivity does not change the total energy storage of the materials, but it can

16   change the thermal storage performance of the materials during certain time duration. For example, the

17   energy efficiency of PCM1$^+$ is 2.7% higher than that of PCM1 and the storage rate of PCM1$^+$ is 30.2%

18   higher in 90 minutes. The decrease of phase transition temperature can significantly improve the heat storage

17

1   efficiency of materials in a short period. For example, the energy efficiency of PCM2 is 4.2% higher than

2   that of PCM1$^+$ within 90 minutes, and the energy storage efficiency of PCM2 is 22.9% higher. As the

3   melting process lasts for longer time, the difference between the thermal conductivity and the phase

4   transition temperature has a smaller effect on the melting process.

5   **3.2.3 exergy storage ratio**

6   The average temperatures varying with charging time for the three materials in the heat storage process

7   are shown in Fig. 9. As can be seen in Fig. 9, due to the influence of thermal conductivity, the temperature

8   rise of PCM1$^+$ is more significant than that of PCM1. Due to the effect of phase transition temperature,

9   although PCM2 has higher efficiency of temperature rise than PCM1, the difference is not large.
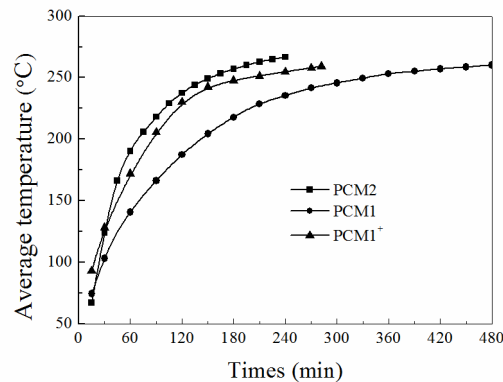
10

11   Fig. 9. Average temperature variation during melting process.

12   According to the Eqs. (11) and (12), the exergy contained in latent heat and sensible heat within 270

13   minutes is calculated. The results are listed in Table 4. The average temperature of PCM1 is 235.429 °C, the

14   average temperature of PCM2 is 266.757 °C, and the average temperature of PCM1$^+$ is 254.648 °C. The

15   temperature of low-temperature heat source is 25 °C. It is shown in Table 4 that PCM2 has the highest

16   capacity of heat to be released and exergy storage efficiency, and the thermal conductivity can improve the

17   heat storage efficiency over a period of time, which is far less than that improved by changing the phase

1   transition temperature.

2   Table 4. The calculated values of heat storage within 270min

Material	Tot. stored (MJ)	Max. stored (MJ)	Exergy storage ratio	Exergy stored/Max. stored energy
PCM1	3.155	3.898	0.809	0.254
PCM2	5.151	5.233	0.984	0.271
PCM1^{+}	3.682	3.898	0.945	0.296

3 \

3.3 The solidification process

7   The liquid fraction, heat transfer flux rate and PCMs average temperature variation are recorded, given

8   the boundary conditions of the solidification process with constant 70 ℃ wall source temperature and 250 ℃

9   initial temperature. The analysis results are described below.

3.3.1 Complete discharging time

11   The liquid fraction variation of three PCMs during the complete solidification process is as shown in

12   Fig. 10. As can be seen in Fig. 10, the liquid phase ratio of PCM1^{+} is always smaller than that of PCM2 at

13   the same time due to the larger phase transition temperature of PCM2. The liquid phase ratio of PCM2 is

14   relatively higher than that of PCM1 in the initial stage, and then, becomes lower. This is because PCM2 has

15   a lower phase transition temperature but a larger thermal conductivity. It also can release more heat in a

16   shorter period so that when the temperature difference reaches a certain level, the liquid phase rate of PCM2

17   is lower than that of PCM1.
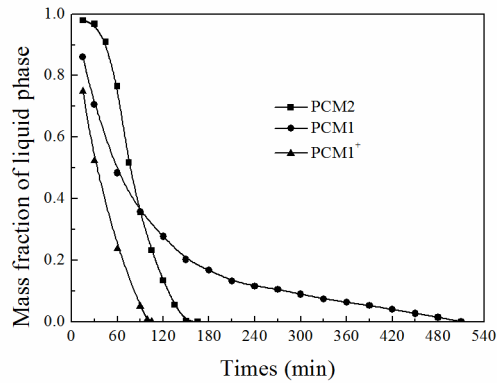
Fig. 10. Mass fraction of liquid fraction variation during solidification process.

3.3.2 Thermal energy release efficiency and ratio

The heat flux curves of three materials is shown in Fig. 11. It can observe in Fig. 11 that the heat transfer rate law in the solidification process is almost consistent with that in the melting process. Because of the phase transition temperature and thermal conductivity, the initial heat transfer power of PCM2 is larger than the others. As the temperature difference between the three PCMs becomes small, the heat transfer power difference decreases.
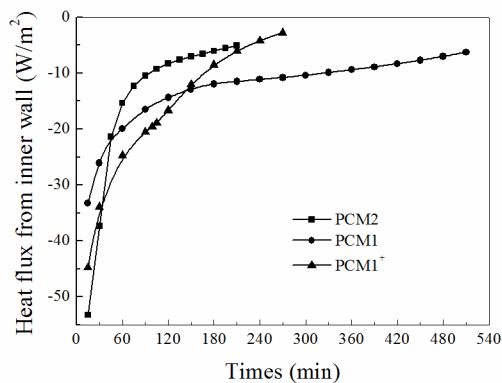
Fig. 11. Heat flux variation from inner wall variation during solidification process.

According to the observations in Fig. 11, the total amount of heat release, heat loss and corresponding heat release efficiency of three PCMs within 105 and 150 minutes (i.e., the complete discharging time of

20

1   PCM2 and PCM1^{+}, respectively) are shown in Tables 5 and 6.

2   Table 5. Calculated thermal energy release and loss within 105 min

Material	Tot. released (MJ)	Heat loss (MJ)	Max. released (MJ)	Energy efficiency	Energy release ratio
PCM1	4.794	0.583	10.545	0.878	0.455
PCM2	10.545	0.471	15.111	0.955	0.698
PCM1[+]	6.169	0.556	10.545	0.910	0.585

3   Table 6. Calculated thermal energy release and loss within 150 min

Material	Tot. released (MJ)	Heat loss (MJ)	Max. released (MJ)	Energy efficiency	Energy release ratio
PCM1	5.661	0.890	10.545	0.843	0.537
PCM2	11.44	0.730	15.111	0.936	0.757
PCM1[+]	8.474	0.832	10.545	0.902	0.804

4   It is shown in Tables 5 and 6 that the heat release rate of PCM2 is significantly higher than that of

5   PCM1^{+} because of its lower phase transition temperature. Although the thermal conductivity can enhance the

6   heat release rate to a certain extent, the influence of this factor is not as significant as the phase transition

7   temperature. At the same time, the thermal conductivity and the phase transition temperature do not affect

8   the heat loss of the simulation area. With the increase of the heat release time, the effect of PCM1^{+} is

9   equivalent to that of PCM2, which means that if the time is long, the influence of phase transition

10   temperature on the heat release efficiency is very low. However, thermal conductivity can promote the

11   efficiency of heat release in long period.

12   **3.3.3 Exergy release ratio**

13   The average temperature curves for three PCMs are provided in Fig. 12. The average temperatures of

14   PCM1, PCM2 and PCM1^{+} are respectively 173.42, 118.59 and 124.55 °C, and the liquid phase rates are

15   0.202, 0 and 0 at the point of 150 minutes in the heat release process. If set the ending time as 105 minutes,

16   the average temperatures corresponding to PCM1, PCM2 and PCM1^{+} are respectively 185.01, 127.13 and

21

1   160.15 °C, and the liquid phase rates are 0.318, 0.232 and 0. Assuming that the cold source reference

2   temperature is 25 °C, the released exergy is given in Tables 7 and 8.
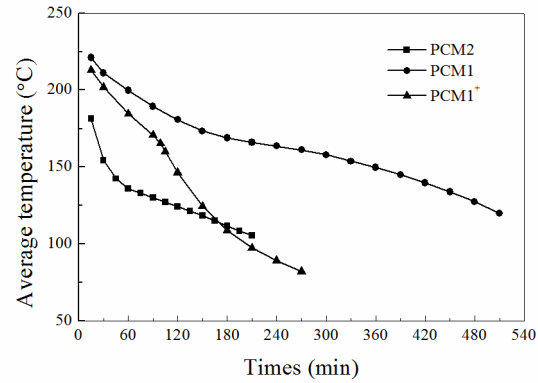
3

4   Fig. 12. Average temperature variation during solidification process.

5   Table 7. Calculated exergy release within 105 min

Material	sensible part (MJ)	latent part (MJ)	Tot. released (MJ)	Ratio of sen./lat.	Max. Released exergy	Ratio of total released /stored
PCM1	1.070	0.809	1.879	1.323	3.496	0.537
PCM2	3.137	0.304	3.441	10.319	4.471	0.770
PCM1$^+$	1.441	1.186	2.627	1.215	3.496	0.751

6   Table 8. Calculated exergy release within 150 min

Material	sensible part (MJ)	latent part (MJ)	Tot. released (MJ)	Ratio of sen./lat.	Max. Released exergy	Ratio of total released /stored
PCM1	1.248	0.946	2.194	1.319	3.496	0.628
PCM2	3.358	0.396	3.754	8.480	4.471	0.840
PCM1$^+$	1.894	1.186	3.08	1.596	3.496	0.881

7   It can be seen in Tables 7 and 8 that the sensible heat release of PCM2 is significantly higher than that

8   of PCM1 while the improvement of the thermal conductivity only has a minor contribution to improving the

9   heat release efficiency when comparing PCM1 and PCM1$^+$. In addition, the phase transition temperature

10   does not affect exergy efficiency much in a short period.

1 **4. Conclusions**

2   This work investigates the combined effect of thermal conductivity and phase transition temperature on

3 SIPH performance, for the purpose of helping select suitable energy storage materials. The influence of

4 thermal conductivity and phase transition temperature of inorganic molten salt PCMs on the LHTES heat

5 transfer characteristics are investigated emphatically. The conclusions are as follows.

6   (1) The proposed numerical simulation model, verified by experimental testing, can provide an efficient

7 and reliable way for heat storage and release performance evaluation.

8   (2) Low phase transition temperature has a significant effect on shortening the complete

9 charging/discharging time in a short period, while have little influence on the heat loss during melting and

10 solidification processes.

11   (3) The high thermal conductivity significantly influences the heat storage and release performance in

12 long-term; however, phase transition temperature nearly has no influence on heat storage/release

13 performance when the process lasts enough time.

14   (4) The comprehensive characteristics of PCM2 are the best among the three PMCs with the lower

15 phase transition temperature and the higher thermal conductivity.

16   However, in the present study we did not provide the optimum values for the phase transition

17 temperature and thermal conductivity of the idea PCM. It is a very challenging task to find the optimal

18 values for the phase transition temperature and thermal conductivity. It should also emphasize that the

19 performance parameters of the materials, heat source, cold source and the production process have much

20 coupling influence on the performance of the LHTES. Future plan will investigate the optimum values of the

21 phase transition temperature and thermal conductivity, and consider the coupling influence of the

22 performance parameters in the LHTES.

6 **References**

7 [1] Farjana S H, Huda N, Mahmud M A P, et al. Solar process heat in industrial systems – A global review.

8   Renewable & Sustainable Energy Reviews, 2017. In Press, https://doi.org/10.1016/j.rser.2017.08.065

9 [2] Sharma A K, Sharma C, Mullick S C, et al. Solar industrial process heating: A review. Renewable &

10   Sustainable Energy Reviews, 2017, 78:124-137.

11 [3] Zalba B, Marín J M, Cabeza L F, et al. Review on thermal energy storage with phase change: materials,

12   heat transfer analysis and applications. Applied thermal engineering, 2003, 23(3): 251-283.

13 [4] da Cunha J P, Eames P. Thermal energy storage for low and medium temperature applications using

14   phase change materials–a review. Applied Energy, 2016, 177: 227-238.

15 [5] Fan L, Khodadadi J M. Thermal conductivity enhancement of phase change materials for thermal

16   energy storage: a review. Renewable and Sustainable Energy Reviews, 2011, 15(1): 24-46.

17 [6] Liu L, Su D, Tang Y, et al. Thermal conductivity enhancement of phase change materials for thermal

18   energy storage: A review. Renewable and Sustainable Energy Reviews, 2016, 62: 305-317.

19 [7] do Couto Aktay K S, Tamme R, Müller-Steinhagen H. Thermal conductivity of high-temperature

20   multicomponent materials with phase change. International Journal of Thermophysics, 2008, 29(2):

21   678-692.

22 [8] Xiao X, Zhang P. Numerical and experimental study of heat transfer characteristics of a shell-tube latent

23   heat storage system: Part I–Charging process. Energy, 2015, 79: 337-350.

24 [9] Wang T, Wang S, Geng L, et al. Enhancement on thermal properties of paraffin/calcium carbonate

25   phase change microcapsules with carbon network. Applied Energy, 2016, 179: 601-608.

[10] Li B, Zhai X. Experimental investigation and theoretical analysis on a mid-temperature solar collector/storage system with composite PCM. Applied Thermal Engineering, 2017, 124:34-43.

[11] Fukai J, Kanou M, Kodama Y, et al. Thermal conductivity enhancement of energy storage media using carbon fibers. Energy Conversion and Management, 2000, 41(14):1543-1556.

[12] Frusteri F, Leonardi V, Vasta S, et al. Thermal conductivity measurement of a PCM based storage system containing carbon fibers. Applied Thermal Engineering, 2005, 25(11): 1623-1633.

[13] Karaipekli A, Biçer A, Sarı A, et al. Thermal characteristics of expanded perlite/paraffin composite phase change material with enhanced thermal conductivity using carbon nanotubes. Energy Conversion and Management, 2017, 134: 373-381.

[14] Zhang P, Ma F, Xiao X. Thermal energy storage and retrieval characteristics of a molten-salt latent heat thermal energy storage system. Applied Energy, 2016, 173: 255-271.

[15] Meng Z N, Zhang P. Experimental and numerical investigation of a tube-in-tank latent thermal energy storage unit using composite PCM. Applied Energy, 2017, 190: 524-539.

[16] Mettawee E B S, Assassa G M R. Thermal conductivity enhancement in a latent heat storage system. Solar Energy, 2007, 81(7): 839-845.

[17] Sciacovelli A, Colella F, Verda V. Melting of PCM in a thermal energy storage unit: Numerical investigation and effect of nanoparticle enhancement. International Journal of Energy Research, 2013, 37(13):1610-1623.

[18] Fan L W, Fang X, Wang X, et al. Effects of various carbon nanofillers on the thermal conductivity and energy storage properties of paraffin-based nanocomposite phase change materials. Applied Energy, 2013, 110: 163-172.

[19] Das N, Kohno M, Takata Y, et al. Enhanced melting behavior of carbon based phase change nanocomposites in horizontally oriented latent heat thermal energy storage system. Applied Thermal Engineering, 2017, 125: 880-890.

[20] Das N, Takata Y, Kohno M, et al. Effect of carbon nano inclusion dimensionality on the melting of phase change nanocomposites in vertical shell-tube thermal energy storage unit. International Journal of Heat and Mass Transfer, 2017, 113: 423-431.

[21] Kousksou T, Strub F, Lasvignottes J C, et al. Second law analysis of latent thermal storage for solar system. Solar Energy Materials & Solar Cells, 2007, 91(14):1275-1281.

[22] Bjurström H, Carlsson B. An exergy analysis of sensible and latent heat storage. Journal of Heat Recovery Systems, 1985, 5(3): 233-250.

[23] Gong Z X, Mujumdar A S. Thermodynamic optimization of the thermal process in energy storage using multiple phase change materials. Applied Thermal Engineering, 1997, 17(11): 1067-1083.

[24] Li Y Q, He Y L, Wang Z F, et al. Exergy analysis of two phase change materials storage system for solar thermal power with finite-time thermodynamics. Renewable Energy, 2012, 39(1):447-454.

[25] Ramayya A V, Ramesh K N. Exergy analysis of latent heat storage systems with sensible heating and subcooling of PCM. International Journal of Energy Research, 2015, 22(5):411-426.

[26] Aldoss T K, Rahman M M. Comparison between the single-PCM and multi-PCM thermal energy storage design. Energy Conversion and Management, 2014, 83: 79-87.

[27] Farid M M, Kim Y, Kansawa A. Thermal performance of a heat storage module using PCM's with different melting temperature: experimental. Journal of Solar Energy Engineering, 1990, 112(2): 125-131.

[28] Zhang P, Xiao X, Meng Z N, et al. Heat transfer characteristics of a molten-salt thermal energy storage unit with and without heat transfer enhancement. Applied Energy, 2015, 137: 758-772.

[29] Q.Peng, J.Ding, X.Wei, et al, The preparation and properties of multi-component molten salts. Applied Energy, 2010, 87(9):2812-2817.

[30] G.Li, Energy and exergy performance assessments for latent heat thermal energy storage systems. Renewable & Sustainable Energy Reviews, 2015, 51:926-954.

[31] Lane G A. Solar heat storage: latent heat materials. Vol.1 Boca Raton, FL: CRC Press, Inc., 1983.

1 **List of figures**

2 **Fig. 1.** Structure diagram of Latent heat thermal energy storage experimental platform.

3 **Fig. 2.** 3D model of LHTES and grid quality analysis of calculation model.

4 **Fig. 3.** Results during melting process

5   (a) Mass fraction of liquid phase contours; (b) Temperature contours.

6 **Fig. 4.** Results during melting process at the location A~F

7   (a) Temperature; (b) Error between ET and ST.

8 **Fig. 5.** Results during solidification process at the location A~F

9   (a)Temperature; (b) Error between ET and ST.

10 **Fig. 6.** Comparison results of the average temperature between ET and ST

11   (a) Melting process;   (b) Solidification process.

12 **Fig. 7.** Mass fraction of liquid fraction variation during melting process.

13 **Fig. 8.** Heat flux variation from inner wall variation during melting process.

14 **Fig. 9.** Average temperature variation during melting process.

15 **Fig. 10.** Mass fraction of liquid fraction variation during solidification process.

16 **Fig. 11.** Heat flux variation from inner wall variation during solidification process

17 **Fig. 12.** Average temperature variation during solidification process.